ACI STRUCTURAL JOURNAL TECHNICAL PAPER

Title No. 121-S22

Shear Strength of Reinforced Concrete Columns with External Post-Tensioned Clamps

by Julian D. Rincon, Yu-Mei Chen, Santiago Pujol, Aishwarya Y. Puranam, and Shyh-Jiann Hwang

An alternative method to retrofit reinforced concrete (RC) columns with insufficient shear reinforcement is investigated. The retrofit involves external prestressing of the columns in the transverse direction to increase both shear strength and drift capacity. External post-tensioned clamps, consisting of high-strength steel rods connecting a set of steel angles, were applied around the columns at different spacings and initial post-tensioning stresses. The tension induced in the steel rods exerts lateral confining pressure on the column by bearing of the angles against the corners of the column. Ten RC columns furnished with external post-tensioned clamps were tested under cyclic loads and approximately constant axial loads. In addition, six RC beams with clamps were tested under monotonically increasing loads. Both the column and beam specimens were fabricated with no transverse reinforcement in the form of conventional steel ties. Therefore, the external clamps were the only source of reinforcement resisting shear. The lateral prestress provided by the clamps was observed to increase the shear stress at the formation of the first inclined crack and at failure. As a result, the mode of failure of columns vulnerable in shear changed from shear failure to a more ductile failure dominated by flexure. The observed increase in shear strength is dependent on the lateral prestress and the tensile strength of the concrete. A simple equation, based on the mechanics of materials, is presented to calculate the shear strength of RC columns with external prestressing.

Keywords: external post-tensioned clamps; lateral prestress; reinforced concrete (RC) columns; retrofit; shear strength.

INTRODUCTION

The work presented in this paper was undertaken to investigate the effects of external prestressing with clamps on the shear strength of reinforced concrete (RC) columns. This report focuses on the ability of clamps to prevent shear failure before flexural yielding of the longitudinal reinforcement. That is one of the most brittle and dangerous modes of failure in RC. It not only affects the ability of the structure to resist strong shaking but also the capacity of the structure to resist its own weight.[1-3] To prevent brittle shear failure, the shear strength of RC members must be designed to exceed the shear demand associated with the flexural strength. Nevertheless, the building stock in seismic regions is heavily populated by buildings that do not meet that demand. Reports of RC building collapses during past earthquakes have identified column failures as one of the primary causes.[4-9] What is more, shear failure of RC columns due to inadequate transverse reinforcement is a recurring observation.

A considerable amount of work on the topic of shear strength of RC for cyclic demands has been done. Yet, the subject is not well understood. Wight and Sozen[10] observed that displacement reversals beyond the yield displacement decrease the shear strength and/or stiffness of RC columns. Loss of shear strength and/or stiffness was related to the formation of inclined cracks, spalling of the concrete cover, expansion of the ties, and loss of interlock resistance of the concrete along inclined cracks. Nonetheless, RC columns with light transverse reinforcement can fail in shear at low drift ratios before yielding of the longitudinal reinforcement.

Recent work by Joint ACI-ASCE Subcommittee 445-B[11,12] suggests that resistance to shear is not affected in a critical fashion by cycles in the linear range of response. That observation reduces the problem of shear failure before flexural yielding to that studied early on by Mörsch[13] and Richart.[14] The literature on the subject of shear failure before flexural yielding is abundant and spans from simple solutions (for example, Richart) to highly elaborate ones (for example, the Modified Compression Field Theory [MCFT][15]). A review of the state of the art was produced by Belarbi et al.[16]

Nevertheless, the scope of these studies has mostly been limited to specimens with conventional ties. Studies of the shear strength of RC columns with post-tensioning transverse reinforcement have been scarce. Two relevant investigations into the topic were carried out by Yamakawa et al.[17] and Skillen.[18] Yamakawa et al.[17] tested 31 small-scale RC columns with widely spaced conventional ties. Of the 31 specimens, 22 were strengthened with post-tensioned external clamps, and the remaining nine had no external clamps. Yamakawa et al.'s test results showed that the post-tensioned clamps were effective in preventing shear failure in the retrofitted columns. Skillen[18] tested two large-scale RC columns to study the effect of lateral pressure by means of external clamps. His proposed clamps were simpler to fabricate and easier to install in comparison with the clamps used by Yamakawa et al. Skillen's test results suggested again that the shear strength of columns with light transverse reinforcement can be increased by applying post-tensioning transverse reinforcement. Still, a number of questions remain. In relation to the work of Yamakawa et al., there are questions about how to extrapolate their results from small-scale columns to full-scale columns with

ACI Structural Journal, V. 121, No. 2, March 2024.

MS No. S-2022-384.R2, doi: 10.14359/51740248, received September 10, 2023, and reviewed under Institute publication policies.

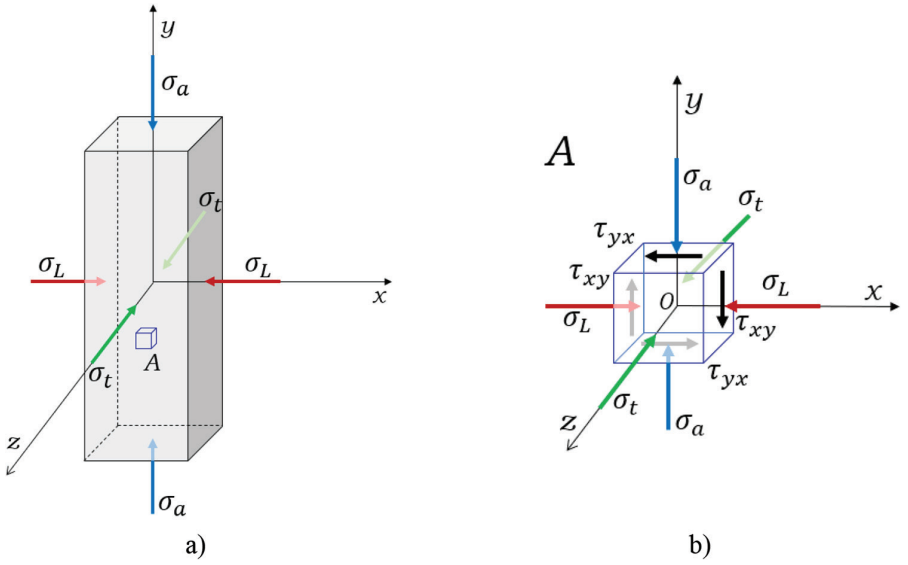

Fig. 1—(a) RC column under axial and lateral stresses; and (b) infinitesimal three-dimensional element oriented to x-y-z-axes. (Note: σ_a is normal longitudinal stress, σ_L is normal transverse stress in parallel direction to x-axis, σ_t is normal transverse stress in parallel direction to z-axis, τ_{xy} is shear stress acting on x-face in direction of y-axis, and τ_{yx} is shear stress acting on y-face in direction of x-axis.)

sizes more representative of what is common in the field. The specimens studied by Skillen were larger, but he tested only two columns, and that is not enough in a problem with as much uncertainty as shear has.

Olesen et al.'s[19] work on the shear of RC beams is of critical relevance to this investigation because it provides a method to consider the effects of lateral prestress on shear strength. Prestressing of concrete structures is generally performed to control flexural cracks and deflections with tendons in the axial direction of a given member. In an attempt to delay the onset and development of shear cracking, tests on columns and beams with post-tensioned transverse reinforcement were conducted at the University of Canterbury (UC) in New Zealand and the National Center for Research on Earthquake Engineering (NCREE) in Taiwan. Lateral prestress was observed to increase the shear stress at the first diagonal cracking and to preclude the formation of large crisscrossing inclined cracks caused by cyclic demands.

RESEARCH SIGNIFICANCE

A method consisting of applying external lateral prestress to retrofit RC columns vulnerable in shear is investigated. The proposed method is easy to design and implement and lends itself as a practical solution for retrofitting large inventories of structures, or in developing countries. Experimental tests conducted on large-scale RC columns showed the effectiveness of external lateral prestress in increasing column shear strength and drift capacity. A simple equation, based on mechanics, for calculating the shear strength of RC columns with lateral prestress is presented.

TECHNICAL FRAMEWORK

The shear strength, denoted as v_c, can be approximated as the shear at the point of first inclined cracking.[14] An expression for the load causing shear cracking in a concrete element

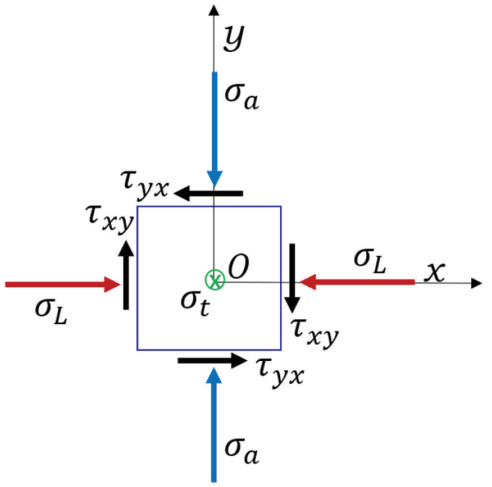

Fig. 2—Two-dimensional view of same element shown in Fig. 1(b).

subjected to lateral prestress is derived using the procedure outlined by Olesen et al.[19]

In Fig. 1(a), an RC column is depicted under axial compressive stress and lateral confinement in two directions perpendicular to its longitudinal axis. In this figure, σ_a is the normal longitudinal stress, σ_L is the normal transverse stress in the x-direction, and σ_t is the normal transverse stress in the z-direction. An infinitesimal element within the column is labeled as "A" and illustrated in Fig. 1(b). A two-dimensional view of element A is presented in Fig. 2. Equilibrium of this element requires the shear stresses τ_{xy} and τ_{yx} to be equal in magnitude and opposite in direction ($\tau_{xy} = \tau_{yx}$). The Mohr's circle in Fig. 3 illustrates the relationship among σ_L, σ_a, and τ_{xy} required for equilibrium.

In Fig. 3, σ_1 and σ_2 represent the maximum and minimum principal stresses, respectively, acting on inclined planes free of shear, as shown in Fig. 4. Compressive stresses are

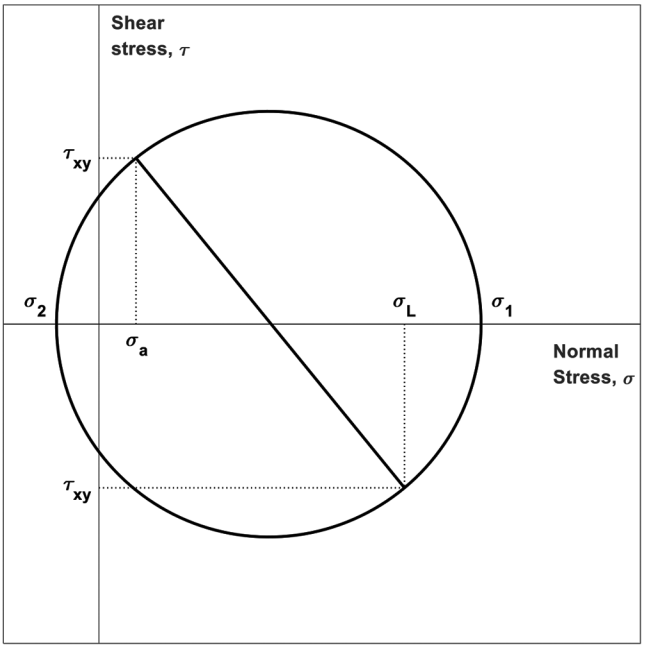

Fig. 3—Mohr's circle corresponding to stresses acting on element shown in Fig. 2.

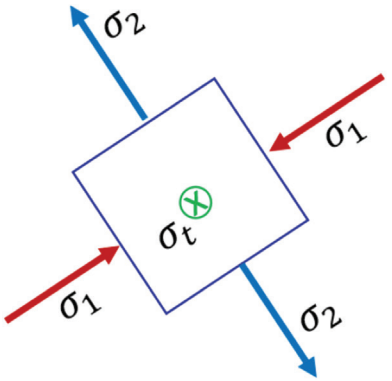

Fig. 4—Principal stresses. (Note: σ_1 is algebraically larger principal stress [compressive stress], σ_2 is algebraically smaller principal stress [tensile stress], and σ_t is normal transverse stress in parallel direction to z-axis.)

drawn as positive, while tensile stresses are drawn as negative. Stress σ_2 is expected to be tensile at inclined cracking.

The principal stresses σ_1 and σ_2 can be calculated using Eq. (1)

$$\sigma_{1,2} = \frac{\sigma_a + \sigma_L}{2} \pm \sqrt{\left(\frac{\sigma_a - \sigma_L}{2}\right)^2 + \tau^2} \quad (1)$$

where σ_1 is the algebraically larger principal stress (compressive stress); σ_2 is the algebraically smaller principal stress (tensile stress); σ_a is the normal longitudinal stress; σ_L is the normal transverse stress in the parallel direction to the x-axis; and τ is shear stress.

In Fig. 5(a), element A is shown on a plane constructed parallel to the directions of stresses σ_1 and σ_t, while Fig. 5(b) illustrates element A on a plane parallel to the directions of stresses σ_2 and σ_t. Notice that the directions parallel to stresses σ_1, σ_2, and σ_t represent the principal stress directions.

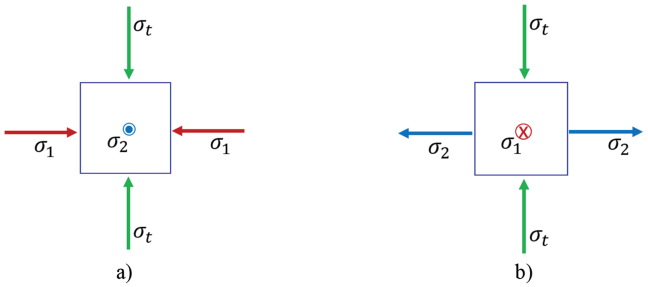

Fig. 5—(a) Stresses seen on plane $\sigma_1 - \sigma_t$; and (b) stresses seen on plane $\sigma_2 - \sigma_t$.

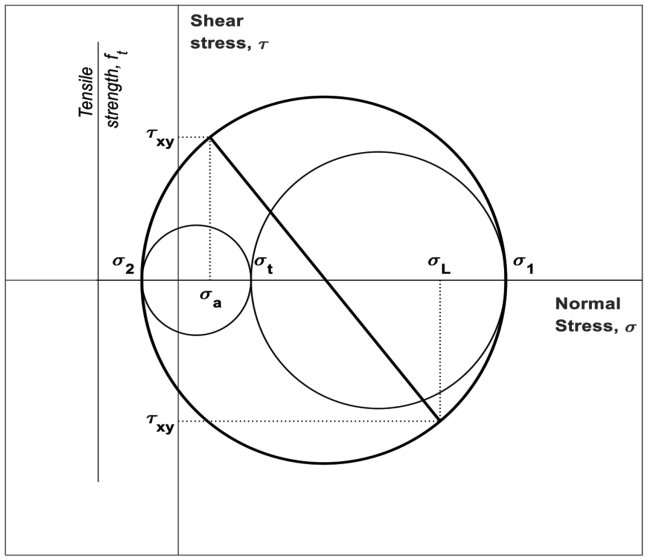

Fig. 6—Mohr's circles for three-dimensional element A shown in Fig. 1.

The corresponding Mohr's circles for these stresses are presented in Fig. 6.

Note that the circles depicted in Fig. 6 are drawn for the case where $\sigma_L > \sigma_t$, with both being compressive stresses. The vertical line on the left represents the tensile strength of the concrete, denoted as f_t. An inclined shear crack is assumed to occur when the principal stress σ_2 exceeds the tensile strength of the concrete f_t. Equating the principal stress σ_2 to the tensile strength f_t gives the following equations for the shear stress in the concrete at inclined cracking.

$$-f_t = \frac{\sigma_a + \sigma_L}{2} - \sqrt{\left(\frac{\sigma_a - \sigma_L}{2}\right)^2 + \tau^2} \quad (2)$$

Solving for τ

$$\tau = f_t \cdot \sqrt{\left(1 + \frac{\sigma_a}{f_t}\right)\left(1 + \frac{\sigma_L}{f_t}\right)} \quad (3)$$

Equation (3) can be rewritten as follows

$$v_c = v_{c_o} \cdot \sqrt{1 + \frac{\sigma_L}{f_t}} \quad (4)$$

where v_c is the shear strength attributable to the concrete in the presence of lateral confining stress σ_L; v_{c_o} is the

Table 1—Specimen details

Specimen	Type of test	Application of P.T.	A.L.R.	a/d	f_c', MPa	$f_t/\sqrt{f_c'}$, MPa	E_c, GPa
C3	C	2	0.15	3.6	30	0.49	21
C5		2			36	0.37	20
C6		2			24	0.46	29
C7		2			26	0.48	32
C8		2			31	0.40	29
C9		2			23	0.40	29
SC1	C	2	0.3	2.2	21	—	—
SC2		2			23	—	—
SC3		2			25	—	—
SC4		2	0.4		25	—	—
B1A	M	N.A.	0	2.2	41	0.53	27
B1B		N.A.	0				
B2A		2	0				
B2B		2	0				
B3A		2	0				
B3B		2	0				
B4A		1	0				
B4B		1	0				
B5A		1	0				
B5B		1	0				
B6A		2	0				
B6B		1	0				

Note: C is cylic; M is monotonic; P.T. is prestress applied in one or two directions; A.L.R. is axial load ratio $P/f_c'A_g$; a/d is shear span-to-effective depth ratio; f_c' is concrete cylinder compressive strength; f_t is concrete tensile strength determined as splitting strength of 100 x 200 mm cylinders; E_c is modulus of concrete.

resistance to shear attributable to concrete in the absence of lateral prestress; σ_L is the lateral confining stress; and f_t is the tensile strength of concrete, and it is assumed to be close to $1/3\sqrt{f_c'}$ MPa.

The primary conclusion drawn from Eq. (4) is that the shear strength attributable to the concrete is proportional to $\sqrt{1+\frac{\sigma_L}{f_t}}$, and this dependence hinges on both the lateral confining stress σ_L and the tensile strength of the concrete f_t.

EXPERIMENTAL DATA

Column tests

Specimen description—Ten RC columns furnished with clamps were tested under displacement reversals and approximately constant axial loads (Tables 1 and 2). Of these 10 columns, six were tested at the Structures Laboratory of UC, and four were tested at NCREE. The UC columns were tested as single-curvature cantilevers, and the NCREE columns were tested in double curvature. Following the nomenclature by Skillen,[18] the UC columns were labeled C3, C5, C6, C7, C8, and C9, and the NCREE columns were labeled SC1, SC2, SC3, and SC4. The test columns at UC were part of a larger project that also included the testing of columns with post-tensioned clamps as a repair measure.[20] Figures 7 to 9 provide details of the columns tested at UC and NCREE. The UC columns had cross-sectional dimensions of 500 x 500 mm, a clear height of 1530 mm, and eight 32 mm diameter longitudinal reinforcing bars. The NCREE columns had cross-sectional dimensions of 750 x 750 mm, a clear height of 3000 mm, and twelve 32 mm diameter longitudinal reinforcing bars. The shear span-to-effective depth ratio (a/d) was 3.6 for UC columns and 2.2 for NCREE columns. The longitudinal reinforcement ratio was approximately 2.6% for UC columns and 1.7% for NCREE columns. All the columns were fabricated with no internal ties. This was done for two reasons: 1) to represent an extreme case of an older RC column with wide tie spacing; and 2) to simplify the estimation of the shear that is resisted by the external transverse reinforcement (clamps). Table 2 summarizes the measured properties of the longitudinal reinforcement and the post-tensioning transverse reinforcement.

At UC, specimens were cast lying on their sides in a single lift and cured for 7 days under plastic, with water dousing occurring during at least the first 3 days. The concrete mixture was supplied by a ready mixed concrete supplier. The cement used was ASTM Type I portland, and the coarse aggregate was a blend of 60% crushed stone (maximum size of 13 mm) and 40% natural alluvial "Greywacke" aggregate (maximum size of 19 mm). The cylinder compressive strength ranged from 21 to 36 MPa.

The specimens at NCREE were also cast on their sides and cured with water dousing three times a day for 7 days. The

Table 2—Longitudinal reinforcement and post-tensioning rods properties

Specimen	Longitudinal reinforcement				Post-tensioning reinforcement				
	A_s, mm^2	ρ_l, %	f_y, MPa	f_u, MPa	A_{pt}, mm^2	s_{pt}, mm	r_{pt}, %	f_{pty}, MPa	f_{ptu}, MPa
C3	6434	2.6	555	698	314	300	0.21	820*	922
C5						200	0.32		
C6						200	0.32		
C7	(8 ϕ 32 mm)				(2 ϕ 16 mm)	300	0.21		
C8						200	0.32		
C9			518	647		300	0.21		
SC1	9651	1.7	466	690	408	200	0.27	1245	1600
SC2						200	0.27		
SC3	(12 ϕ 32 mm)				(2 ϕ 18 mm)	300	0.18		
SC4						200	0.27		
B1A	982	2.0	550	680	57	—	0	—	—
B1B						—	0	—	—
B2A						95	0.3	260	369
B2B						95	0.3		
B3A						143	0.2		
B3B						143	0.2		
B4A	(2 ϕ 25 mm)				(2 ϕ 6 mm)	143	0.2	290	452
B4B						143	0.2		
B5A						95	0.3	289	468
B5B						95	0.3	290	452
B6A						190	0.15	290	468
B6B						190	0.15		

*For clamps with no welds (as in C3), nominal resistance to shear provided by clamps is inferred to be close to $v_s = r_{pt} \cdot 0.6 f_{pty}$ instead of $v_s = r_{pt} \cdot f_{pty}$.

Note: A_s is total area of longitudinal reinforcement; ρ_l is longitudinal reinforcement ratio; f_y is longitudinal reinforcement yield stress; f_u is longitudinal reinforcement ultimate stress; A_{pt} is area of post-tensioning transverse reinforcement (one clamp, two legs); s_{pt} is spacing of clamps; r_{pt} is reinforcement ratio of post-tensioning transverse reinforcement; f_{pty} is post-tensioning transverse reinforcement yield stress; f_{ptu} is post-tensioning transverse reinforcement ultimate stress.

concrete mixture was supplied by a ready mixed concrete supplier. The cement used was ASTM Type I portland. The nominal coarse aggregate size was 19 mm. The cylinder compressive strength ranged from 21 to 25 MPa.

External post-tensioned clamps on columns

The clamps studied are similar to those used by Skillen.[18] They consisted of four corner brackets, each made with pairs of steel angles, and high-strength threaded rods connecting the brackets (Fig. 10). A key difference from the clamps used by Skillen[18] is that the clamps used in this study were welded. Welding was applied to prevent the concentration of shear force in rods. Welding can be avoided if the clamps are sized assuming their strength is controlled by the rod sections working in shear. That is, $v_s = r_{pt} \cdot 0.6 f_{pty}$ instead of $v_s = r_{pt} \cdot f_{pty}$.

For the tests at UC, clamps were fabricated with 16 mm thick angles and 16 mm diameter threaded rods with a measured yield stress of 820 MPa. The spacing between clamps s_{pt} was either 200 or 300 mm (Table 3). The post-tensioned transverse reinforcement area ratio r_{pt}, calculated using Eq. (5), was 0.21 or 0.32%. The initial prestress in the threaded rods f_{pti} ranged from $0.1 f_{pty}$ (low prestress) to $0.7 f_{pty}$ (high prestress), where f_{pty} is the yield stress of the threaded rods. The equivalent lateral confining stress caused by the clamps on the column σ_L is expressed as the transverse reinforcement ratio times the initial prestress in the clamps, and it is calculated using Eq. (6). This stress ranged from 0.2 to 1.7 MPa.

For the tests at NCREE, clamps were fabricated with 25 mm thick angles and 18 mm diameter threaded rods with a mean measured yield stress of 1250 MPa. The spacing between clamps s_{pt} was 200 or 300 mm (Table 3). The post-tensioned transverse reinforcement area ratio r_{pt} was 0.18 or 0.27%. The initial prestress in the threaded rods ranged from $0.1 f_{pty}$ to $0.55 f_{pty}$. The equivalent lateral confining stress caused by the clamps on the column σ_L ranged from 0.3 to 1.8 MPa

$$r_{pt} = \frac{A_{pt}}{b \cdot s_{pt}} \tag{5}$$

$$\sigma_L = r_{pt} \cdot f_{pti} \tag{6}$$

where r_{pt} is the post-tensioned transverse reinforcement area ratio; A_{pt} is the total area of post-tensioned transverse reinforcement within spacing s_{pt}; b is the width of

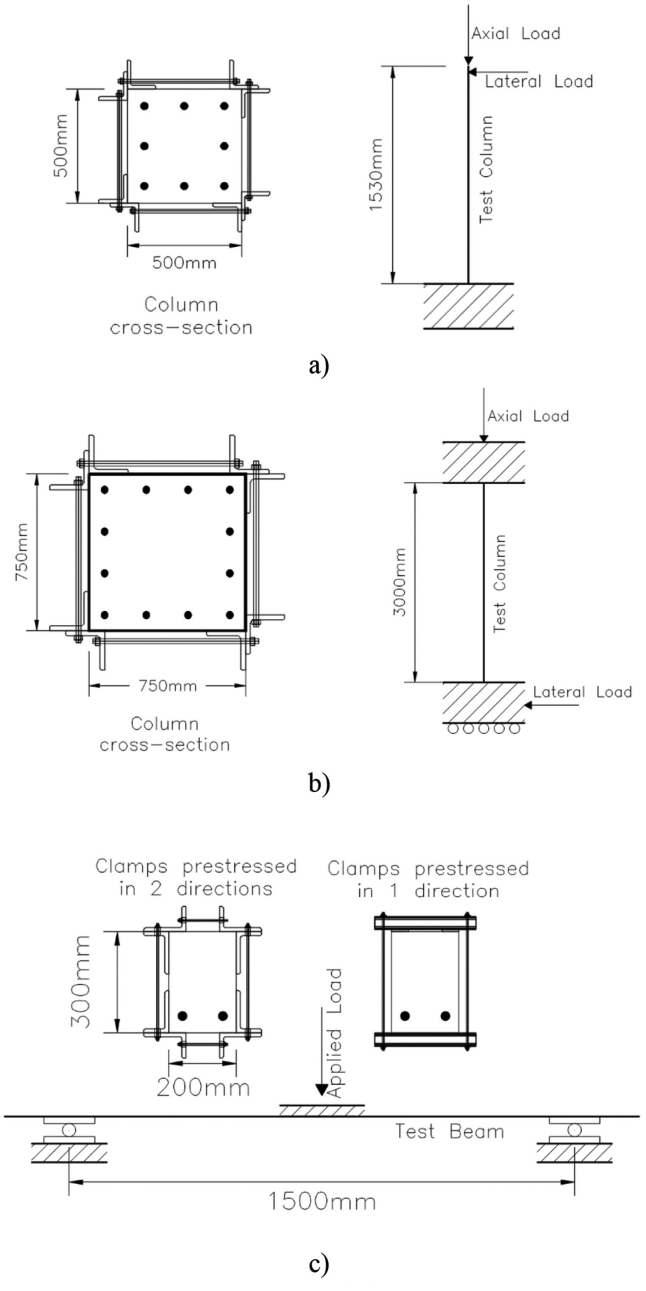

Fig. 7—Typical dimensions: (a) columns at UC; (b) columns at NCREE; and (c) beams.

the compression face of the column; s_{pt} is the spacing of post-tensioned transverse reinforcement; σ_L is the lateral confining stress caused by the clamps; and f_{pti} is the initial prestress in the clamps.

Application of clamps—Pairs of steel angles were positioned at the four corners of the concrete column and connected to each other with steel threaded rods. All rods were equipped with load cells, placed between the steel angle and a 12 mm thick washer (Fig. 11). Clamps with low initial prestress were snug-tightened using a spanner. In contrast, for clamps with intermediate or high prestress ($f_{pti} > 0.4f_{pty}$), additional force was applied using a hydraulic bolt tensioner. Gradual increments in force, following a crisscross tightening sequence, ensured even forces in the rods and prevented rotation of the clamps.

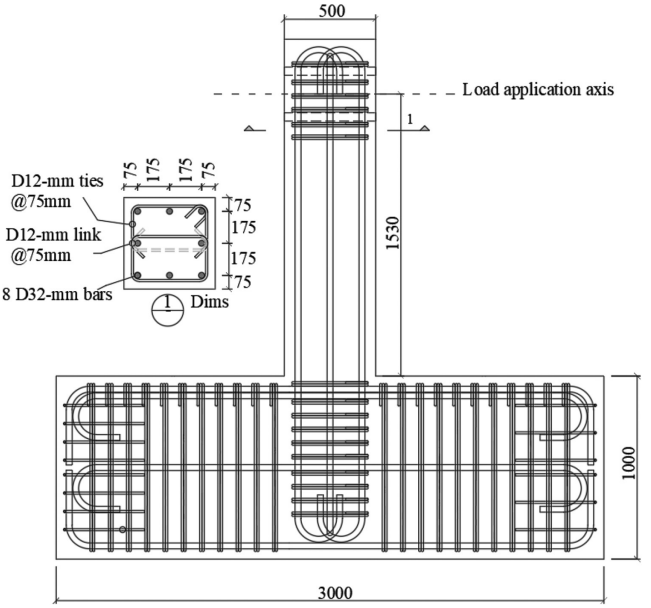

Fig. 8—Details of columns tested at UC.

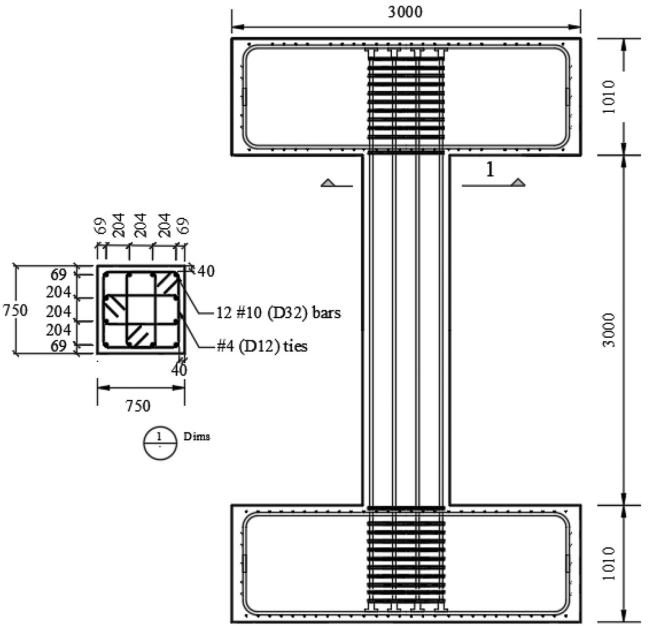

Fig. 9—Details of columns tested at NCREE.

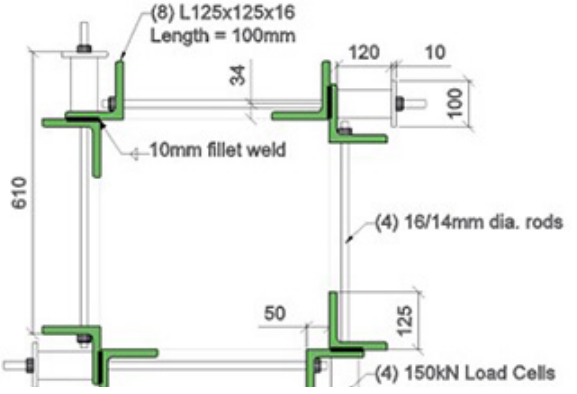

Fig. 10—Post-tensioned clamps applied on column.

Table 3—Summary of test results

Specimen	f_c', MPa	A.L.R.	P.T.	s_{pt}, mm	s_{pt}/d	r_{pt}, %	σ_L, MPa	v_c, MPa	$v_c/\sqrt{f_c'}$, MPa	v_{max}, MPa	v_s, MPa	$(v_{max} - v_s)$, MPa	$(v_{max} - v_s)/\sqrt{f_c'}$, MPa
C3	30	0.15	2	300	0.71	0.21	0.2	1.5	0.27	2.3	—	—	—
C5	36		2	200	0.47	0.32	0.3	1.9	0.32	2.7	—	—	—
C6	24		2	200	0.47	0.32	1.7	2.2	0.45	2.5	—	—	—
C7	26		2	300	0.71	0.21	0.7	1.9	0.37	2.5	—	—	—
C8	31		2	200	0.47	0.32	1.0	2.2	0.39	2.5	—	—	—
C9	23		2	300	0.71	0.21	1.1	2.0	0.42	2.5	—	—	—
SC1	21	0.3	2	200	0.29	0.27	0.3	2.0	0.44	2.9	—	—	—
SC2	23		2	200	0.29	0.27	1.8	2.9	0.62	3.2	—	—	—
SC3	25		2	300	0.44	0.18	1.2	2.5	0.51	3.1	—	—	—
SC4	25	0.4	2	200	0.29	0.27	1.8	3.1	0.64	3.5	—	—	—
B1A	41	0	—	—	—	0	0.0	1.8	0.30	2.0	0	2.0	0.30
B1B		0	—	—	—	0	0.0	1.8	0.27	2.1	0	2.1	0.27
B2A		0	2	95	0.38	0.3	0.0	1.7	0.27	2.9	1.11	1.8	0.28
B2B		0	2	95	0.38	0.3	0.6	2.0	0.31	3.6	1.11	2.5	0.55
B3A		0	2	143	0.57	0.2	0.0	1.8	0.28	2.5	0.74	1.8	0.39
B3B		0	2	143	0.57	0.2	0.4	2.3	0.37	3.2	0.74	2.5	0.50
B4A		0	1	143	0.57	0.2	0.0	1.8	0.28	2.8	0.90	1.9	0.30
B4B		0	1	143	0.57	0.2	0.5	—	0.34	3.8	0.90	2.9	0.59
B5A		0	1	95	0.38	0.3	0.8	2.1	0.31	3.4	1.40	2.0	0.34
B5B		0	1	95	0.38	0.3	0.0	2.0	0.33	3.6	1.36	2.2	0.32
B6A		0	2	190	0.76	0.15	0.4	2.0	0.31	2.7	0.70	2.0	0.31
B6B		0	1	190	0.76	0.15	0.4	2.1	0.33	2.8	0.70	2.1	0.33

Note: f_c' is concrete cylinder compressive strength; A.L.R. is axial load ratio $P/f_c'A_g$; P.T. is prestress applied in one or two directions; s_{pt} is spacing of clamps; d is effective depth, distance from centroid of exterior layer of longitudinal steel to outermost fiber in compression; r_{pt} is reinforcement ratio of post-tensioning transverse reinforcement; σ_L is lateral confining stress caused by clamps on column; v_c is shear stress at inclined cracking; v_{max} is maximum measured shear stress; v_s is shear strength contribution of transverse reinforcement, calculated as $v_s = r_{pt} \cdot f_{ptu}$ (applicable to beams only).

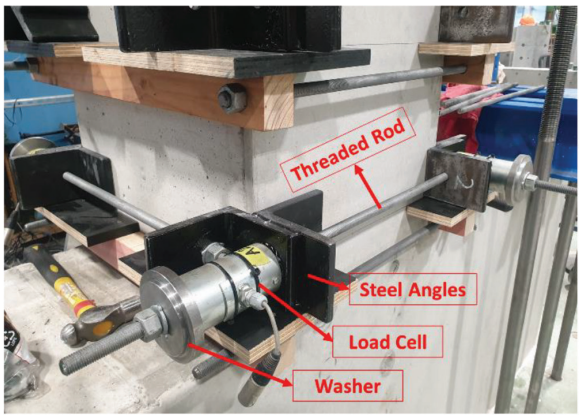

Fig. 11—Application of clamps.

Procedure for column tests

Figures 12(a) and (b) show the test setup at UC and NCREE, respectively. The axial load ratio (A.L.R. = $P/A_g f_c'$) was 0.15 for columns tested at UC and 0.3 (SC1, SC2, and SC3) or 0.4 (SC4) for columns tested at NCREE. The loading protocol is shown in Fig. 13. Three cycles were applied at each drift ratio. Testing was paused at points of peak displacement and zero lateral load to record data. Cracks were marked at each peak displacement. Testing concluded when the peak lateral load in a given cycle was less than 50% of the maximum.

Beam tests

Specimen description—Six simply supported RC beams furnished with clamps were tested under monotonic loads applied at midspan (Tables 1 and 2). Figures 7 and 14 show typical details of the beam specimens. The test beams had cross-sectional dimensions of 200 x 300 mm, with a distance between support centerlines of 1500 mm. The clear distance between support faces was 550 mm. Longitudinal reinforcement consisted of two 25 mm diameter steel bars with a measured yield stress of 550 MPa (averaging results from three coupons). The longitudinal reinforcement ratio was 2%. The effective depth, defined as the distance from the centroid of the exterior layer of longitudinal steel to the outermost fiber in compression, was 250 mm. The a/d was 2.2.

All six beams were cast from a single batch of concrete. After the concrete set, wet hessian cloth (burlap) and plastic were placed over the beams. Curing lasted for 7 days, with water dousing occurring once a day. The formwork was stripped after 3 days of casting. At 28 days, the measured compressive cylinder strength was 41 MPa on average. The

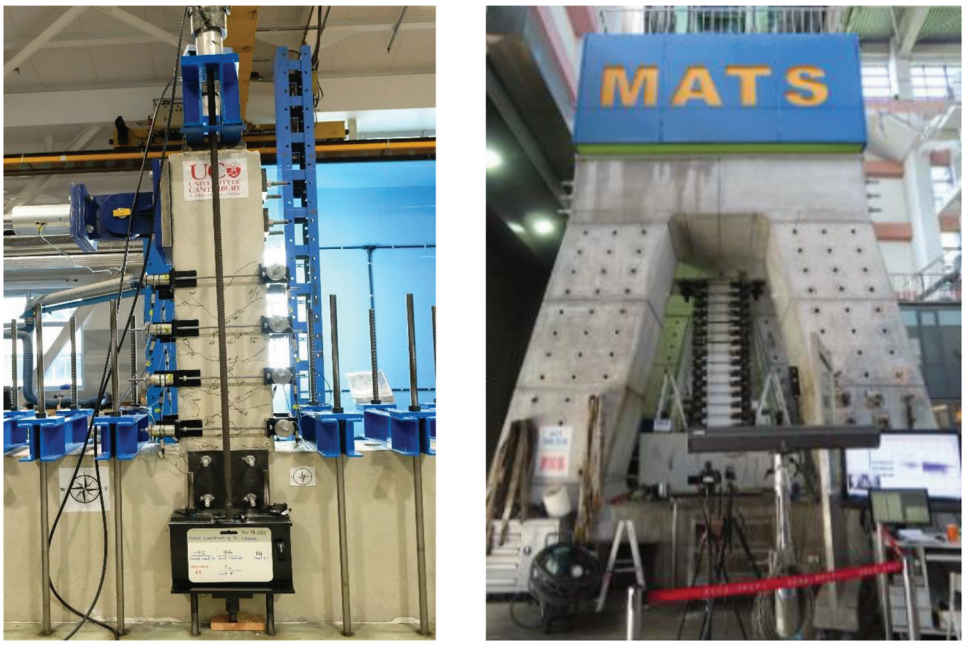

a) b)

Fig. 12—Test setup at: (a) UC; and (b) NCREE.

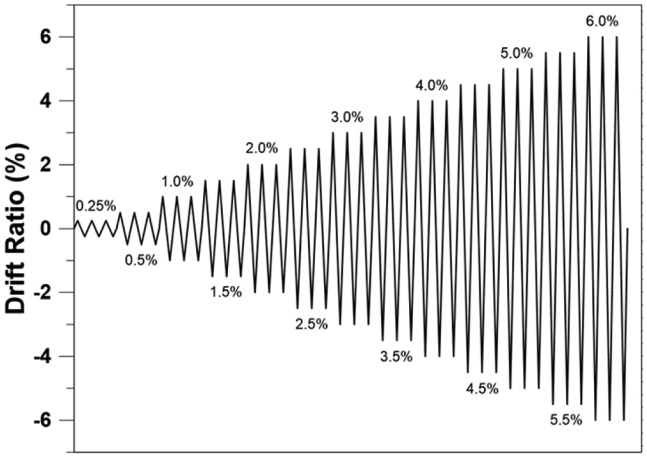

Fig. 13—Loading protocol for columns.

concrete cylinders were kept under the same curing conditions as the beams and were also cured for 7 days, with water dousing occurring simultaneously with the beams.

Similar to the columns, the test beams were fabricated with no conventional stirrups, with post-tensioning being the only source of steel resisting shear. The nominal resistance to shear v_n was calculated using Eq. (7), which is based on observations made by Richart.[14] Equation (7) expresses the nominal resistance to shear v_n as the sum of contributions to shear attributed to the concrete v_c and the transverse reinforcement v_s.

$$v_n = v_c + v_s \tag{7}$$

The test beams were designed to fail in shear. In all cases, the nominal resistance to shear v_n was smaller than the calculated unit plastic shear stress v_p. The unit plastic shear stress is associated with the shear force at flexural yielding V_p. This force is obtained from a sectional moment analysis (Eq. (8) to (10)). The calculated shear plastic stress v_p for measured properties was 3.8 MPa.

To obtain the contribution to the shear resistance of the concrete v_c, in the absence of lateral prestress, one beam without clamps was tested (B1). The concrete resistance to shear v_c averaged 1.8 MPa from tests of each beam span B1A and B1B. The remaining five beams were furnished with clamps at different spacings s_{pt} and, by varying the initial prestress in the clamps, different lateral confining pressures. The nominal shear resistance provided by the clamps ranged from 0.7 MPa (for beams B6A and B6B) to 1.4 MPa (for beam B5A)

$$M_p = A_s \cdot f_y \cdot j \cdot d \tag{8}$$

$$V_p = \frac{M_p}{a^*} \tag{9}$$

$$v_p = \frac{V_p}{b \cdot d} \tag{10}$$

where M_p is the moment at flexural yielding at the critical section; A_s is the cross-sectional area of the reinforcing bars; f_y is the measured yield stress of the longitudinal reinforcement; j is the ratio of the internal lever arm to the effective depth (assumed as 0.9); d is the effective depth; V_p is the shear force associated with M_p; a^* is the distance from center of roller supports to face of midspan loading plate (in beams); v_p is the unit shear stress associated with V_p; and b is the column width.

External post-tensioned clamps on beams

Two types of clamps were used for the RC beam tests: clamps applying prestress in one or two directions (Fig. 14). Table 1 provides information on the beams tested with prestress applied in one or two directions. Clamps applying

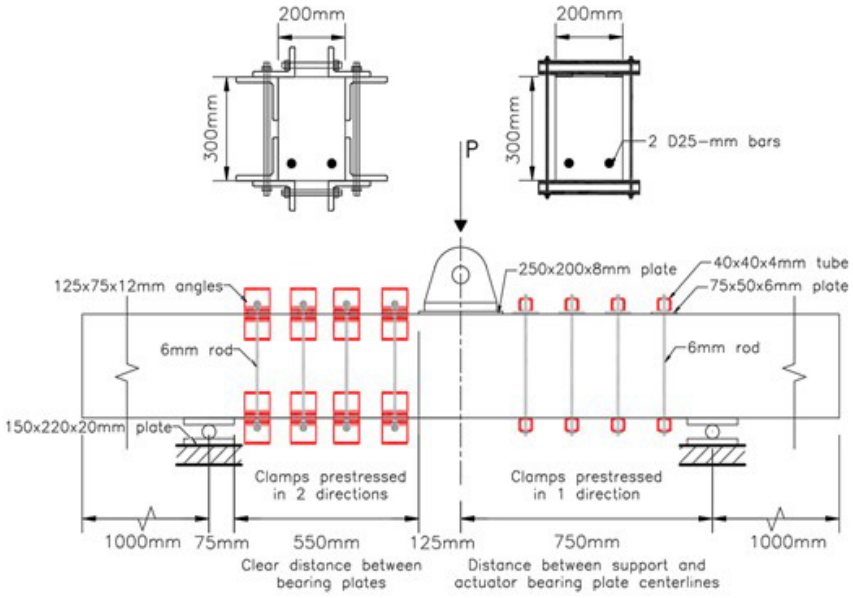

Fig. 14—Details of beams.

prestress in one direction, parallel to the applied force, were fabricated from 40 x 40 x 4.0 mm rectangular hollow tubes, 6 mm diameter threaded rods, and 75 mm wide bearing steel plates. The plates were placed on the face of the beam in compression, and their width matched the size of the two-directional clamps. Clamps applying prestress in two directions were similar to the clamps used for columns. They consisted of 12 mm thick angles and 6 mm diameter threaded rods. The measured ultimate stress of the threaded rods ranged from 368 to 468 MPa. The spacing of the clamps s_{pt} ranged from 95 to 143 mm ($0.38 < s_{pt}/d < 0.76$). The post-tensioned transverse reinforcement area ratio r_{pt}, calculated using Eq. (5), ranged from 0.15 to 0.3%. The lateral confining stress caused by the clamps on the beam σ_L, calculated using Eq. (6), ranged from 0 to 0.8 MPa.

Procedure for beam tests

Each beam underwent two tests (tests A and B), resulting in a total of 12 tests. Heavy-size clamps were applied to one side of the beam, aiming to induce failure on the opposite side. The shear strength contribution of the heavy clamps was 4.5 MPa, which was approximately 1.2 times the calculated shear stress v_p at yielding of the longitudinal reinforcement. On the opposite side of the beam, either no clamps, as in the case of the bare beam (tests B1A and B1B), or smaller clamps were installed. Figure 15 illustrates the beam specimen with heavy clamps on one side and smaller clamps on the other side. The applied load was increased in steps of approximately 10 kN. After each load increment, cracks were marked and measured. This process continued until shear failure occurred on one side of the beam. Subsequently, the heavy clamps were relocated to the failed side, and the beam underwent testing again.

Fig. 15—Test setup for beams.

EXPERIMENTAL RESULTS AND DISCUSSION

Results from columns

Hysteretic response—Table 3 provides a summary of the test results. The hysteretic responses for all the columns are shown in Fig. 16 and 17. Figure 16 focuses on the columns tested at UC. In this figure, the top three plots correspond to columns with a transverse reinforcement area ratio of 0.21% (clamps spaced at 300 mm) but with different initial post-tensioning stresses. Column C3 had clamps with low initial prestress ($f_{pti} = 0.1f_{pty}$), C7 had intermediate initial prestress ($f_{pti} = 0.4f_{pty}$), and C9 had high initial prestress ($f_{pti} = 0.7f_{pty}$), resulting in equivalent σ_L values of 0.2, 0.7, and 1.1 MPa, respectively.

Moving to the bottom three plots in Fig. 16, these show the response of columns with a transverse reinforcement area ratio of 0.32% (clamps spaced at 200 mm). Columns C5, C8, and C6 had clamps with low, intermediate, and high initial prestress, respectively, resulting in equivalent σ_L values of 0.3, 1.0, and 1.7 MPa.

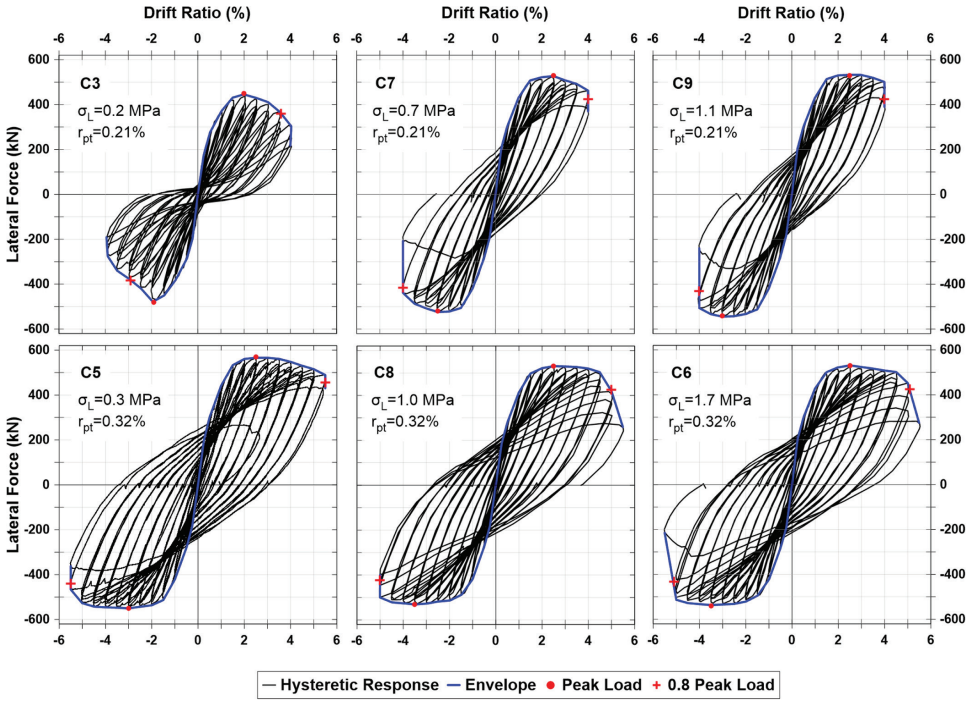

Fig. 16—Hysteretic response of columns tested at UC.

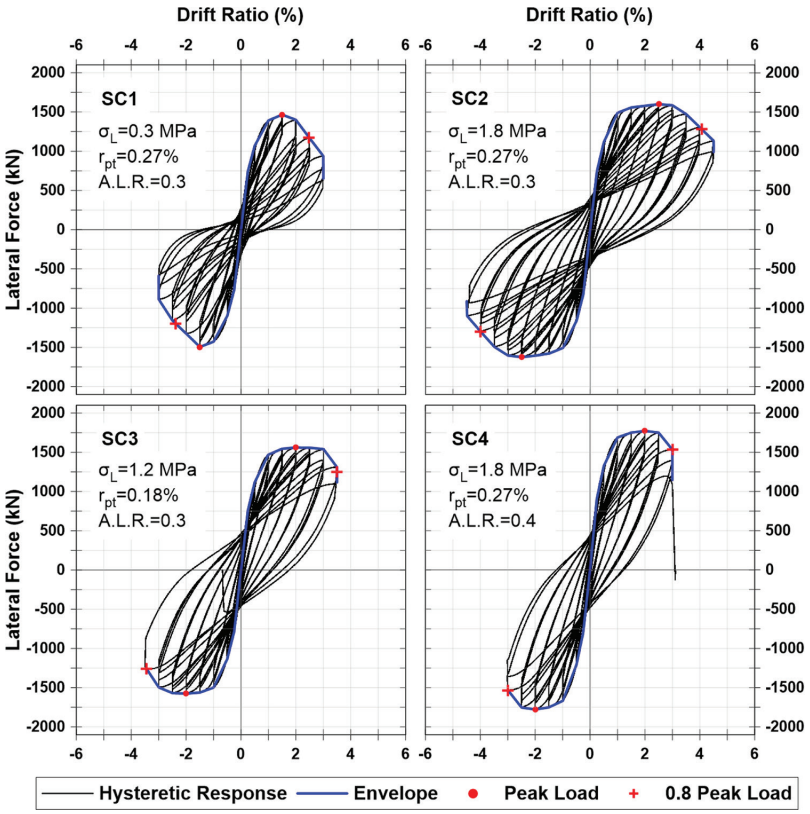

Fig. 17—Hysteretic response of columns tested at NCREE.

These data suggest that an increase in initial prestress led to a more ductile column response. For instance, Column C3 exhibited shear disintegration of the concrete core, while the response of C9 was dominated by flexure with a larger drift capacity.

All the columns but C3 reached flexural yielding. Having no welds in clamps, C3 did not yield in flexure because its nominal shear strength was close to $v_c + r_{pt} \cdot 0.6f_{pty}$ (instead of $v_c + r_{pty} \cdot f_y$), which is smaller than the unit shear associated with flexural yielding. For all other columns, yielding occurred at a drift ratio of approximately 1.5%. The peak measured load was 525 kN on average, and the associated shear stress was 2.5 MPa. Table 4 lists the measured peak loads and drift capacities for all 10 columns. The peak

loads reported in Table 4 represent the maximum shear forces applied in both pushing and pulling directions. Drift capacity is defined as the drift that the column reaches before its lateral load resistance drops to 80% of the maximum measured load. Testing concluded when the peak lateral load in a given cycle was less than 50% of the maximum.

Figure 17 shows the response from columns tested at NCREE. Column SC1 had clamps with low initial prestress ($f_{pti} = 0.1f_{pty}$), while SC2, SC3, and SC4 had clamps with intermediate initial prestress ($f_{pti} = 0.55f_{pty}$). The transverse reinforcement area ratio was 0.18% for SC3 and 0.27% for the other columns. The lateral confining stress σ_L, calculated using Eq. (6), was 0.3, 1.8, 1.2, and 1.8 MPa for SC1, SC2, SC3, and SC4, respectively.

Table 4—Peak loads and drift capacities

Specimen	f_c', MPa	r_{pt}, %	σ_L, MPa	Peak loads		D.C., %
				Pushing direction, kN	Pulling direction, kN	
C3	30	0.21	0.2	450	480	3.0
C5	30	0.32	0.3	570	550	5.5
C6	24	0.32	1.7	530	540	5.0
C7	26	0.21	0.7	530	520	4.0
C8	31	0.32	1.0	530	530	5.0
C9	23	0.21	1.1	530	540	4.0
SC1	21	0.27	0.3	1465	1495	2.5
SC2	23	0.27	1.8	1600	1625	4.0
SC3	25	0.18	1.2	1560	1575	3.5
SC4	25	0.27	1.8	1770	1780	3.0

Note: f_c' is concrete cylinder compressive strength; r_{pt} is reinforcement ratio of post-tensioning transverse reinforcement; σ_L is lateral confining stress caused by clamps; D.C. is drift capacity, defined as drift ratio associated with 20% decrease in lateral load resistance of column. It is calculated with help of envelope of load-displacement loops. Two values of drift capacities are obtained (pulling and pushing directions), but only smaller value is reported.

All the columns reached yielding of the longitudinal reinforcement at a drift ratio of approximately 1.2%. The measured peak loads ranged from 1465 to 1780 kN. Differences in peak loads were likely due to the applied lateral prestress, ranging from 0.3 to 1.8 MPa, and the higher axial load ($0.4A_gf_c'$) in SC4. Table 4 shows the peak loads and drift capacities.

Clamp stress—Forces in the clamps were measured at one end of each threaded rod using load cells. Clamp stresses were calculated as the measured force divided by the net rod cross-sectional area (approximately 80% of the gross area; refer to Table 2). Figure 18 presents a graphical representation of clamp stresses measured in the test of SC1. The figure includes data for the first three clamps positioned at the ends of the column. Each curve in the figure shows the change in the stress in threaded rods parallel to the applied lateral force. The markers on the curves represent measurements taken at peak displacements during the first cycle at each displacement target. Note that each curve has a different origin on the horizontal axis, and the spacing between vertical gridlines corresponds to 100 MPa. The vertical axis represents the applied unit shear stress V/bd divided by $\sqrt{f_c'}$, where V is the applied lateral force, b is the width of the column or dimension perpendicular to the direction of the applied force, d is the effective depth of the column, and f_c' is the concrete cylinder compressive strength on the day of testing in MPa.

All the curves in Fig. 19 show no change in clamp stress before the applied shear stress exceeded a threshold. This threshold indicates the formation of inclined cracks and has been assumed to be a reasonable approximation of the contribution to shear strength attributable to the concrete v_c. Changes in clamp stress after inclined cracking were more noticeable in columns with low initial prestress. These

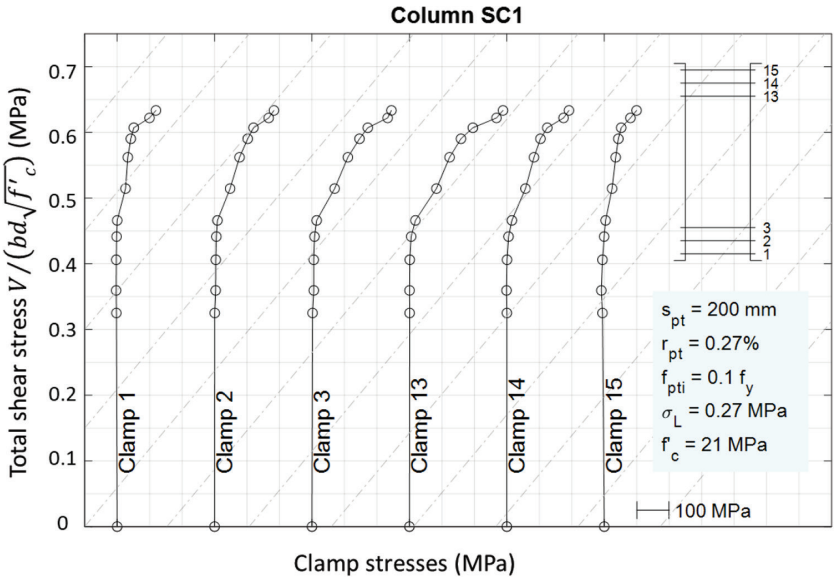

Fig. 18—Total shear stress versus stress in key clamps, Column SC1. (Note: s_{pt} is spacing between clamps, r_{pt} is post-tensioned transverse reinforcement area ratio, f_{pti} is initial prestress in clamps [as fraction of yield stress of high-strength rods f_{pty}], σ_L is lateral prestress caused by clamps on column, and f_c' is measured concrete cylinder strength at test day.)

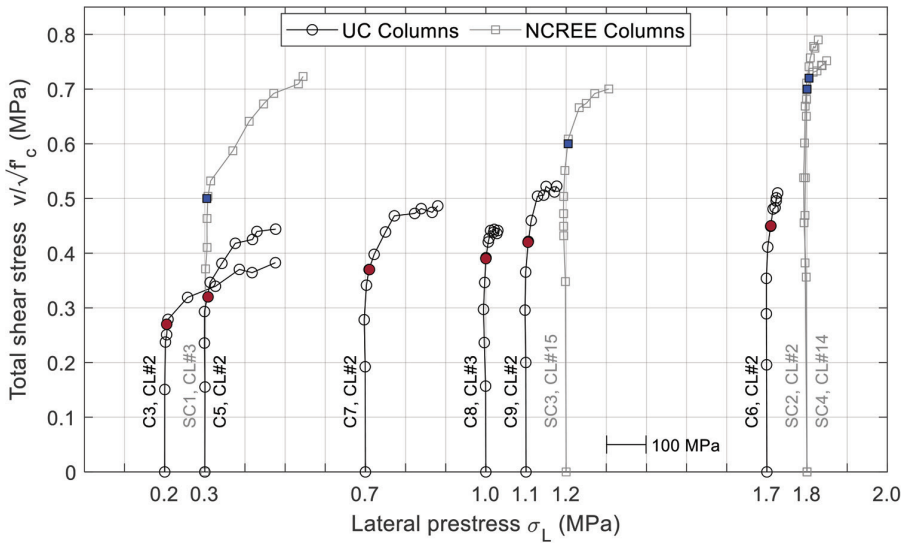

Fig. 19—Shear stress versus clamp stresses (selected clamps).

Table 5—Applied shear stress and clamp stresses, in MPa

C3		C5		C6		C7		C8		C9		SC1		SC2		SC3		SC4	
$v/\sqrt{f_c'}$	Clamp No. 2	$v/\sqrt{f_c'}$	Clamp No. 2	$v/\sqrt{f_c'}$	Clamp No. 2	$v/\sqrt{f_c'}$	Clamp No. 2	$v/\sqrt{f_c'}$	Clamp No. 3	$v/\sqrt{f_c'}$	Clamp No. 2	$v/\sqrt{f_c'}$	Clamp No. 3	$v/\sqrt{f_c'}$	Clamp No. 2	$v/\sqrt{f_c'}$	Clamp No. 15	$v/\sqrt{f_c'}$	Clamp No. 14
0.00	0	0.00	0	0.00	0	0.00	0	0.00	0	0.00	0	0.00	0	0.00	0	0.00	0	0.00	0
0.15	0	0.16	0	0.20	–1	0.19	–1	0.16	–1	0.20	–1	0.33	2	0.34	–5	0.31	–2	0.31	–2
0.24	2	0.24	–1	0.29	–1	0.28	–3	0.24	–4	0.30	–3	0.36	6	0.41	–5	0.38	–6	0.40	–7
0.25	5	0.29	–1	0.35	–1	0.34	3	0.30	–6	0.37	–1	0.41	5	0.47	–4	0.40	–6	0.47	–8
0.28	8	0.35	13	0.41	2	0.37	9	0.35	–3	0.42	6	0.44	8	0.57	–2	0.42	–6	0.53	–6
0.32	57	0.38	42	0.45	9	0.40	22	0.39	0	0.46	13	0.47	14	0.60	–1	0.44	–6	0.59	–4
0.34	126	0.42	76	0.48	15	0.44	50	0.42	6	0.50	29	0.52	70	0.62	–1	0.49	–3	0.63	–1
0.37	186	0.43	119	0.48	20	0.47	72	0.43	8	0.51	44	0.56	111	0.64	15	0.54	5	0.65	5
0.36	218	0.44	130	0.50	24	0.47	123	0.44	12	0.52	50	0.59	146	0.65	25	0.59	33	0.67	8
0.38	276	0.44	176	0.50	23	0.48	139	0.44	19	0.51	71	0.61	172	0.66	36	0.59	50	0.69	17
—	—	—	—	0.51	27	0.47	166	0.44	21	0.5225	76	0.63	233	0.65	37	0.61	71	0.68	20
—	—	—	—	—	—	0.49	180	0.44	28	—	—	0.64	245	0.66	49	0.62	106	0.70	28
—	—	—	—	—	—	—	—	0.44	30	—	—	—	—	—	—	—	—	—	—

Note: v is shear stress, calculated as V/b_d; V is applied shear force; b is width of column; d is effective depth, distance from centroid of exterior layer of longitudinal steel to outermost fiber in compression; f_c' is concrete cylinder compressive strength.

changes accelerated as applied shear stress increased. The slope of the curves relating applied shear stress and clamp stress approached r_{pt}, as observed by Richart.[14] For columns with clamps with initial prestress $f_{pti} > 0.4f_{pty}$, the applied shear stress causing the first variation in clamp stress was less clear. Larger lateral prestress σ_L not only caused an increase in the shear at inclined cracking but also a reduction in the width and length of inclined cracks. Inclined cracks not forming as extensions of flexural cracks were not observed in columns with $\sigma_L > 1.7$ MPa ($0.3\sqrt{f_c'}$). As a consequence, estimating v_c from clamp-stress measurements was more difficult for specimens C6, SC2, and SC4 (where σ_L was at least 1.7 MPa). Approximate estimates of the shear stress at inclined cracking (assumed to represent v_c) were obtained from Fig. 19. Each curve in this figure represents the variation of clamp stress with increases in applied shear stress for the most critical clamp in each of the 10 test columns. The distance between vertical gridlines (100 MPa) represents the increase in clamp stress. The horizontal distance between the origin of each curve and the y-axis represents the initial lateral prestress σ_L. Curve labels indicate the specimen ID and clamp number. Colored markers indicate points chosen to represent the formation of inclined cracks, with y-coordinates representing estimates of v_c. These points were chosen considering these criteria:

- Focus on clamps between $d/2$ and d from column ends;
- Consider rods parallel to the applied shear force;
- Identify a noticeable increase in clamp stress;
- Compare the slope of the shear stress-clamp stress curve with the transverse reinforcement area ratio r_{pt}; and
- Corroborate the presence of inclined cracks in photos taken when the mentioned stresses were measured.

All stresses illustrated in Fig. 19 are listed in Table 5 to allow the reader to plot the data and select different estimates for v_c if deemed necessary.

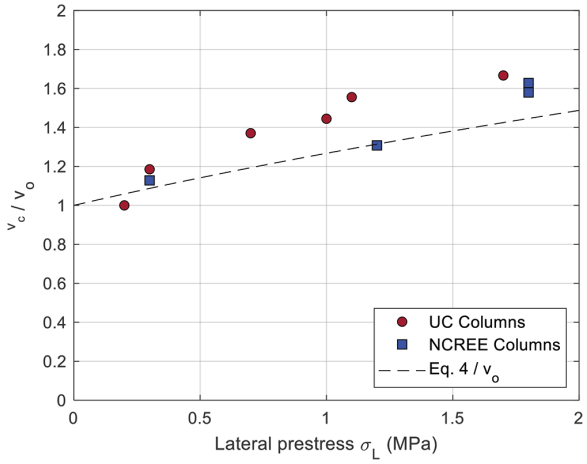

Fig. 20—Concrete shear stress versus lateral prestress.

The estimates of v_c obtained from Fig. 19 are plotted again versus the initial lateral prestress σ_L in Fig. 20, with shear stress normalized relative to a reference shear stress v_o. This reference stress is meant to represent the shear strength of a column without lateral prestress and without ties. Because shear strength is expected to be sensitive to differences in axial load and reinforcement ratio, two values of v_o were used: $0.4\sqrt{f_c'}$ MPa for the columns tested at NCREE (with $0.3 < P/A_g f_c' < 0.4$), and $0.27\sqrt{f_c'}$ MPa for the columns tested at UC ($P/A_g f_c' = 0.15$). For each column set, the reference value v_o was obtained as the intercept with the y-axis of a regression line fitted through the colored markers in Fig. 19. Figure 20 shows that v_c, as defined here, increased with increasing initial lateral prestress σ_L. Equation (4) produced a lower-bound estimate for this increase. The largest deviations from Eq. (4) occurred for columns with large initial lateral prestress in which detecting the formation of inclined cracks was more difficult.

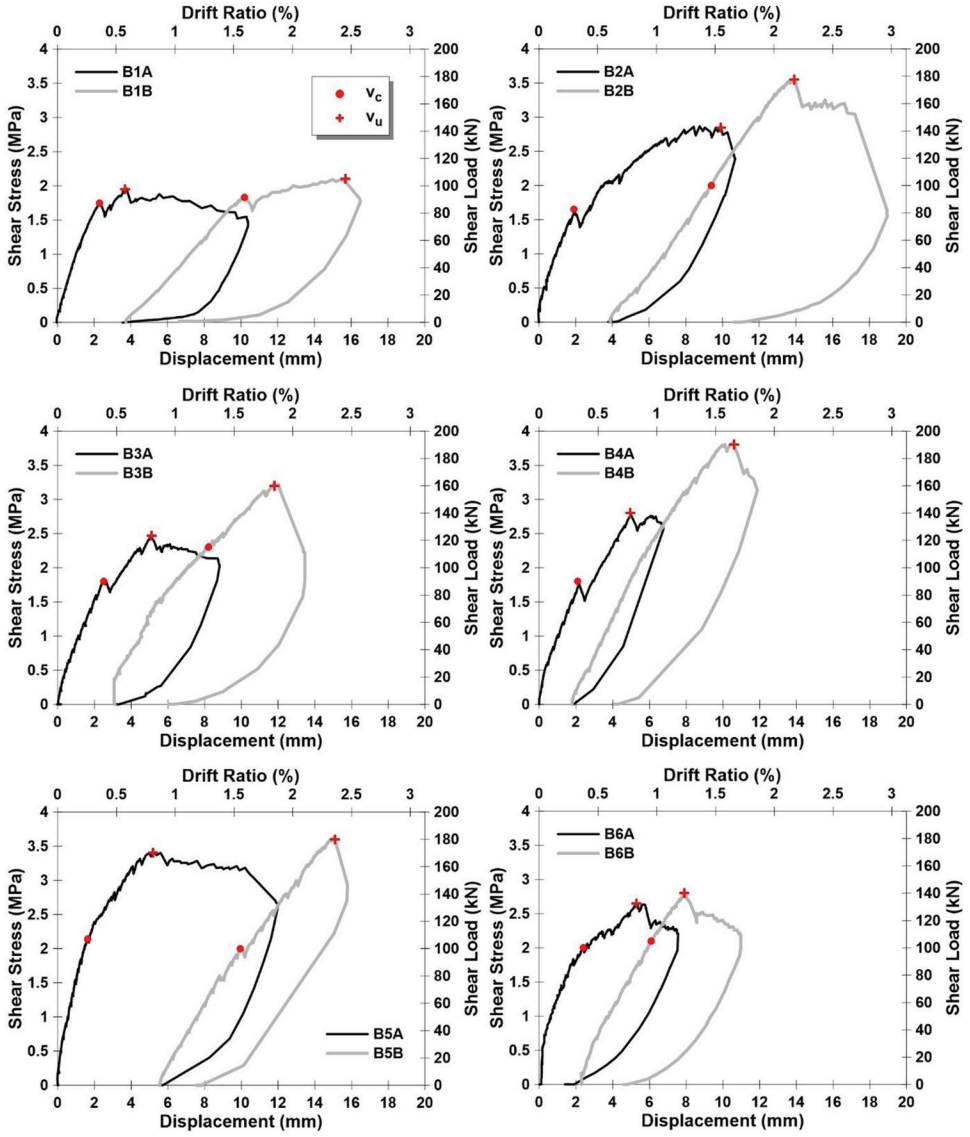

Fig. 21—Load versus deflection curves of beams.

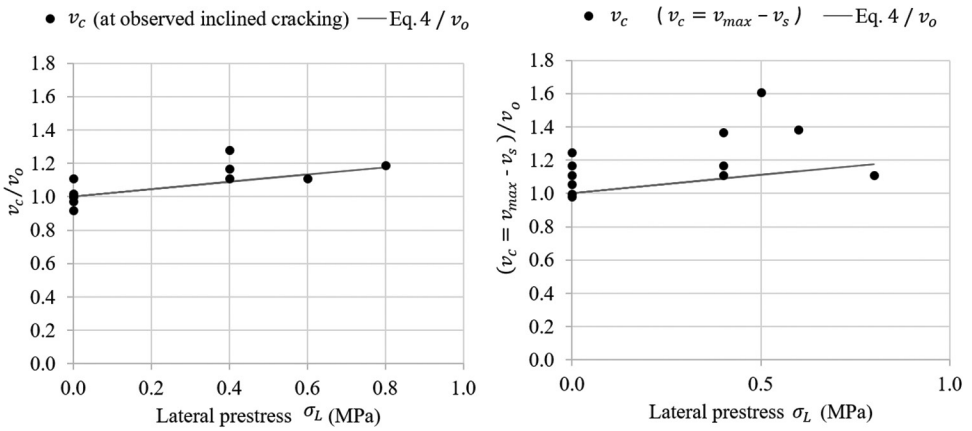

Fig. 22—Variations in v_c*: (a) at observed inclined cracking; and (b) calculated as* $v_{max} - v_s$.

Results from beams

Table 3 summarizes the test results. The load-deflection curves for all the beams are shown in Fig. 21. The objective of the beam tests was to study whether the increase in shear stress at inclined cracking observed in the column tests leads to a similar increase in monotonic shear strength. For this purpose, the test beams were proportioned to fail in shear before yielding in flexure. In all beams with clamps, shear failure occurred by fracture of the threaded rods after the formation of a large inclined crack in the beam.

Clamps installed on the beams were not instrumented. Therefore, the estimation of the load at inclined cracking relied purely on visual observation. Except for test 4B, in which a clear observation was not obtained, the load at inclined cracking was clearly identified—to the best judgment of the writers—during each beam test. Assuming that the shear at inclined cracking and the contribution to shear strength attributable to the concrete are similar to one another, the former was compared with the difference between the total shear measured at failure v_{max} and the contribution to shear strength attributed to the clamps v_s. Table 3 shows: a) the shear stresses at inclined cracking; b) the total shear stress at failure v_{max}; and c) v_s obtained as the reinforcement ratio times the measured rod strength f_{ptu}. Figure 22(a) illustrates variations in shear stress at observed inclined cracking with increasing values of σ_L. Figure 22(b) illustrates variations in $v_{max} - v_s$ with increasing values of σ_L. The similarities between these two figures suggest that increases in shear stress at inclined cracking caused by increases in initial lateral prestress translated into similar increases in shear strength (for monotonically increased shear). In addition, Fig. 23 shows that increases in shear stress at inclined cracking observed in beams were comparable to those observed in columns even in beams with initial lateral prestress in a single direction (parallel to the applied force), supporting Eq. (4) and the aforementioned theoretical framework.

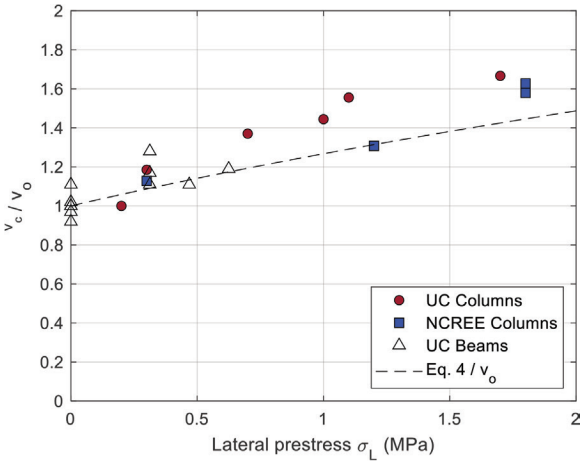

Fig. 23—Concrete shear stress versus lateral prestress (including beams).

CONCLUSIONS

- Observations made by Richart[14] on reinforced concrete (RC) beams with conventional ties led him to propose Eq. (7) (that is, $v_n = v_c + v_s$). Equation (7) expresses the nominal resistance to shear v_n as the contribution to shear resistance attributable to the concrete v_c and the contribution attributable to the transverse reinforcement v_s. Although Eq. (7) was originally derived for RC beams with conventional ties, acceptable results were obtained assuming that post-tensioned clamps resist shear in a similar fashion to conventional ties.
- The shear strength attributable to the concrete v_c, interpreted as the shear at the formation of the first inclined crack, was observed to be nearly proportional to $\sqrt{1 + \frac{\sigma_L}{f_t}}$, where σ_L represents the lateral prestress, and f_t stands for the tensile strength of the concrete, assumed to be close to $1/3\sqrt{f_c'}$ in MPa. It follows that a high value of σ_L can delay the formation of shear inclined cracks. The beam tests showed an increase in v_c at both inclined cracking and failure.
- The increase in the concrete resistance to shear v_c in the beams was observed to be unaffected by whether prestress was applied solely in the loading direction or in both the loading and transverse directions. This observation is in agreement with the Mohr's circle shown in Fig. 6. Confining stresses transverse to the loading direction (σ_t) are not expected to provide an additional benefit to the shear strength attributable to the concrete v_c.

- The proposed post-tensioned clamps can be used as an effective method to retrofit non-ductile RC columns with insufficient transverse reinforcement. The introduction of post-tensioned clamps prevented non-ductile columns from shear failure before flexural yielding.

ACKNOWLEDGMENTS

This study was supported by QuakeCoRE (New Zealand Centre for Earthquake Resilience) at the University of Canterbury and NCREE (National Center for Research on Earthquake Engineering) at the National Taiwan University. The first writer is thankful to the Resilience to Nature's Challenges Project for the 3-year postgraduate scholarship awarded. The writers also acknowledge the support received from the laboratory technicians: G. Keats, T. O'Connell, T. Perigo, J. Maley, D. Carney, and M. Weavers; as well as from the undergraduate students: B. Bassett-Foss, A. Meneghini, J. Wight, J. Carlielle, J. Redfern, and E. Osborn as part of their end-year project for the BE(Hons) degree in civil engineering.

AUTHOR BIOS

ACI member **Julian D. Rincon** *is a PhD Candidate in earthquake engineering at the University of Canterbury, Christchurch, New Zealand. He received his BS from the University of Valle, Cali, Colombia. His research interests include the seismic performance of structures and the repair and retrofit of reinforced concrete structures.*

ACI member **Yu-Mei Chen** *is a Graduate Student in the Department of Civil Engineering at National Taiwan University, Taipei, Taiwan.*

Santiago Pujol, *FACI, is a Professor of civil engineering at the University of Canterbury. He is Chair of ACI Committee 133, Disaster Reconnaissance; Vice Chair of ACI Subcommittee 445-B, Shear & Torsion-Seismic Shear; and a member of ACI Committee 314, Simplified Design of Concrete Buildings; ACI Subcommittees 318-F, Foundations, and 318-1W, Wind Provisions; and Joint ACI-ASCE Committee 445, Shear and Torsion. He received his BS from the National University of Colombia, Bogotá, Colombia, and his MS and PhD from Purdue University, West Lafayette, IN. His research interests include displacement-based design of earthquake-resistant structures, instrumentation, monitoring, repair and strengthening of structures, and engineering data management.*

ACI member **Aishwarya Y. Puranam** *is an Assistant Professor in the Department of Civil Engineering at National Taiwan University. She received her BSCE, MSCE, and PhD from Purdue University in 2013, 2016, and 2018, respectively. She is a member of ACI Committee 133, Disaster Reconnaissance. Her research interests include the behavior of reinforced concrete structures subjected to seismic demands, large-scale experiments, and data preservation.*

ACI member **Shyh-Jiann Hwang** *is a Professor in the Department of Civil Engineering at National Taiwan University. He received his PhD from the University of California, Berkeley, Berkeley, CA. He is a member of Joint ACI-ASCE Committee 352, Joints and Connections in Monolithic Concrete Structures. His research interests include the shear behavior of reinforced concrete members and seismic design and retrofitting of reinforced concrete structures.*

REFERENCES

1. Elwood, K. J., and Moehle, J. P., "Axial Capacity Model for Shear-Damaged Columns," *ACI Structural Journal*, V. 102, No. 4, July-Aug. 2005, pp. 578-587.

2. Henkhaus, K. W., "Axial Failure of Vulnerable Reinforced Concrete Columns Damaged by Shear Reversals," PhD dissertation, Purdue University, West Lafayette, IN, 2010.

3. Li, Y.-A.; Weng, P.-W.; and Hwang, S.-J., "Seismic Performance of Reinforced Concrete Intermediate Short Columns Failed in Shear," *ACI Structural Journal*, V. 116, No. 3, May 2019, pp. 195-206. doi: 10.14359/51713309

4. Hanson, R. D., and Degenkolb, H. J., *The Venezuela Earthquake, July 29, 1967*, American Iron and Steel Institute, Washington, DC, 1969, 176 pp.

5. Muguruma, H.; Nishiyama, M.; and Watanabe, F., "Lessons Learned from the Kobe Earthquake—A Japanese Perspective," *PCI Journal*, V. 40, No. 4, July-Aug. 1995, pp. 28-42.

6. Lew, H. S.; Leyendecker, E. V.; and Dikkers, R. D., "Engineering Aspects of the 1971 San Fernando Earthquake," Building Science Series No. 40, National Bureau of Standards, Washington, DC, 1971, 412 pp.

7. Yurdakul, Ö.; Duran, B.; Tunaboyu, O.; and Avşar, Ö., "Field Reconnaissance on Seismic Performance of RC Buildings after the January 24, 2020 Elazığ-Sivrice Earthquake," *Natural Hazards*, V. 105, No. 1, Jan. 2021, pp. 859-887. doi: 10.1007/s11069-020-04340-x

8. Milićević, I.; Marinković, M.; Blagojević, N.; and Nikolić-Brzev, S., "Performance of RC Frames in 26.11.2019. Albania Earthquake: Effects of Irregularities and Detailing," *Građevinski Materijali i Konstrukcije*, V. 64, No. 3, Aug. 2021, pp. 207-213.

9. Gautam, D.; Rodrigues, H.; Bhetwal, K. K.; Neupane, P.; and Sanada, Y., "Common Structural and Construction Deficiencies of Nepalese Buildings," *Innovative Infrastructure Solutions*, V. 1, No. 1, 2016, Article No. 1, 18 pp. doi: 10.1007/s41062-016-0001-3

10. Wight, J. K., and Sozen, M. A., "Shear Strength Decay in Reinforced Concrete Columns Subjected to Large Deflection Reversals," Engineering Experiment Station, University of Illinois Urbana-Champaign, Urbana, IL, Aug. 1973, 312 pp.

11. Usta, M.; Alhmood, A.; Carrillo, J.; Cladera, A.; Laughery, L.; Pujol, S.; Puranam, A.; Rautenberg, J.; Sezen, H.; Sneed, L. H.; and To, D. V., "Shear Strength of Structural Walls Subjected to Load Cycles," *Concrete International*, V. 41, No. 5, May 2019, pp. 42-48.

12. Shrestha, S.; Carrillo, J.; Sezen, H.; and Pujol, S., "Shear Strength of Shear-Controlled Columns under Cyclic Loading," *ACI Structural Journal*, V. 119, No. 3, May 2022, pp. 129-140.

13. Mörsch, E., "Der Eisenbetonbau seine Theorie und Anwendung," Konrad Wittwer GmbH & Co., Stuttgart, Germany, 1908, 376 pp. (in German)

14. Richart, F. E., "An Investigation of Web Stresses in Reinforced Concrete Beams," Bulletin No. 166, Engineering Experiment Station, University of Illinois Urbana-Champaign, Urbana, IL, June 1927, 106 pp.

15. Vecchio, F. J., and Collins, M. P., "The Modified Compression-Field Theory for Reinforced Concrete Elements Subjected to Shear," *ACI Journal Proceedings*, V. 83, No. 2, Mar.-Apr. 1986, pp. 219-231.

16. Belarbi, A.; Kuchma, D. A.; and Sanders, D. H., "Proposals for New One-Way Shear Equations for the 318 Building Code," *Concrete International*, V. 39, No. 9, Sept. 2017, pp. 29-32.

17. Yamakawa, T.; Kamogawa, S.; and Kurashige, M., "Seismic Performance and Design of RC Columns Retrofitted by PC Bar Prestressing as External Hoops," *Journal of Structural and Construction Engineering (Transactions of AIJ)*, V. 65, No. 537, 2000, pp. 107-113.

18. Skillen, K. C., "The Effects of Transverse Reinforcement on the Strength and Deformability of Reinforced Concrete Elements," PhD dissertation, Purdue University, West Lafayette, IN, 2020, 368 pp.

19. Olesen, S. E.; Sozen, M. A.; and Siess, C. P., "Investigation of Prestressed Reinforced Concrete for Highway Bridges: Part IV: Strength in Shear of Beams with Web Reinforcement," Structural Research Series No. 295, Engineering Experiment Station, University of Illinois Urbana-Champaign, Urbana, IL, Aug. 1965, 162 pp.

20. Rincón, J., and Pujol, S., "Retrofit and Repair of Reinforced Concrete Columns with Active Confinement," *Proceedings of the 2023 New Zealand Society for Earthquake Engineering Annual Technical, Conference*, Auckland, New Zealand, 2023, Paper No. 34, 10 pp.

REGISTER TODAY

TECHNOLOGY FORUM

MAY 14-16, 2024, SANTA FE, NM, USA

Hilton Santa Fe - Historic Plaza, 100 Sandoval Street

The **Technology Forum** is an innovation-focused educational and networking event for concrete professionals **powered by the ACI Foundation's Concrete Innovation Council**.

Whether you are an emerging professional or a seasoned veteran, the ACI Foundation Technology Forum is the place to learn about **current trends, emerging technologies, and discoveries within the concrete industry**.

Join us for an exciting and insightful event featuring thought leaders and technology innovators to discuss the future of the concrete industry.

aci Foundation
Building the Future

acifoundation.org